

On the relationship between the H₂ emission and the physical structure of planetary nebulae

R. A. Marquez-Lugo,¹★ G. Ramos-Larios,¹ M. A. Guerrero² and R. Vázquez³

¹*Instituto de Astronomía y Meteorología, Av. Vallarta No. 2602, Col. Arcos Vallarta, C.P. 44130 Guadalajara, Jalisco, Mexico*

²*Instituto de Astrofísica de Andalucía, IAA-CSIC, C/ Glorieta de la Astronomía s/n, E-18008 Granada, Spain*

³*Instituto de Astronomía, Universidad Nacional Autónoma de México, Apdo. Postal 877, 22800 Ensenada, B.C., Mexico*

Accepted 2012 November 6. Received 2012 November 5; in original form 2012 October 1

ABSTRACT

Mid-infrared (IR) observations of planetary nebulae (PNe) have revealed diffuse emission associated with their main nebular shells and outer envelopes or haloes. The interpretation of this emission is uncertain because the broad-band mid-IR images may include contributions of different components. In particular, the *Spitzer* Infrared Array Camera 8 μm images, that best reveal these nebular features, can include contributions not only of H₂ lines, but also those of ionic species, polycyclic aromatic hydrocarbon features and thermal dust continuum emission. To investigate the nature of the emission detected in mid-IR observations of a sample of 10 PNe, we have obtained narrow-band near-IR H₂ $\lambda 2.122 \mu\text{m}$ and optical [N II] $\lambda 6584 \text{ \AA}$ images. The comparison between these images confirms that a significant fraction of the emission detected in the IRAC 8 μm images can be attributed to molecular hydrogen, thus confirming the utility of these mid-IR images to investigate the molecular component of PNe. We have also detected H₂ emission from PNe whose physical structure cannot be described as bipolar, but rather as ellipsoidal or barrel like. These detections suggest that, as more sensitive observations of PNe in the H₂ $\lambda 2.122$ line are acquired, the detection of H₂ emission is not exclusive of bipolar PNe, although objects with this morphology are still the brightest H₂ emitters. Finally, we remark that the bright H₂ emission from the equatorial ring of a bipolar PN does not arise from a photodissociation region shielded from the ultraviolet stellar radiation by the ring itself, but from dense knots and clumps embedded within the ionized material of the ring.

Key words: ISM: jets and outflows – ISM: lines and bands – infrared: ISM.

1 INTRODUCTION

Molecular hydrogen (H₂) can be expected in the photodissociation regions (PDR) of planetary nebulae (PNe), where the expanding envelope sweeps up the wind from the progenitor asymptotic giant branch (AGB) star. Molecular hydrogen can also form in neutral clumps embedded within the ionization zone, where high extinction, high density and molecular (and dust) shielding allow H₂ to survive from the stellar radiation (McCandliss et al. 2007). The H₂ molecules in PNe can be excited by the ultraviolet (UV) radiation field of their central stars (CSPNe) in the photodissociation front (Black & van Dishoeck 1987) or by shocks (Burton, Hollenbach, & Tielens 1992). It has been suggested recently that H₂ can originally form in an excited state (Aleman & Gruenwald 2011).

It has been traditionally assumed that H₂ emission arises from regions where material is predominantly molecular. Therefore, it is not surprising that H₂ emission is mainly detected at the equatorial

regions of bipolar PNe,¹ because their thick equatorial discs would shield the UV radiation of the PN central star (CSPN), allowing the survival of H₂ molecules (Kastner et al. 1996; Guerrero et al. 2000). Furthermore, the confinement of bipolar PNe to low Galactic latitudes has made them suspected to descend from the population of most massive progenitor stars of PNe (Corradi & Schwarz 1995). As these stars would eject thicker and more massive envelopes, this is considered an additional argument linking bipolar morphology with the significant presence of molecular material (Peimbert & Torres-Peimbert 1983; Hora & Latter 1996). The strong correlation between H₂ emission and bipolar morphology has originated the so-called *Gatley's rule* (Kastner et al. 1994): ‘the detection of the 2.122 μm S(1) line of H₂ is sufficient to determine the bipolar nature of a PN’.

¹ Hereafter we will adopt the definition of bipolar PNe given by Corradi & Schwarz (1995) as those whose H α images display ‘an equatorial waist from which two faint, extended bipolar lobes depart’. When the morphology of the PN was insufficient to determine its physical structure (a ring-like PN can be interpreted as a pole-on bipolar source), we will rely only on kinematical information of the source.

★ E-mail: alejmar@astro.iam.udg.mx

The increase in sensitivity of near- and mid-infrared (IR) observations of H₂ lines (Hora 2006) and the access to other wavelength ranges [e.g. far-UV by the *Far-UV Spectroscopic Explorer (FUSE)*] have revealed the presence of molecular hydrogen in PNe with a variety of morphologies (Dinerstein, Sterling & Bowers 2006). The wavelength range between 1 and 10 μm is especially relevant because it includes a large number of transitions of molecular hydrogen (Turner & Zuckerman 1977). The intensity line ratios of some of these lines (the 2–1 S(1) λ2.2477/1–0 S(1) λ2.1218 and 1–0 S(0) λ2.2235/1–0 S(1) λ2.1218 particularly) can be used to infer the molecular excitation mechanism (shocks or UV radiation field) and the physical conditions of H₂ (see Likkel et al. 2006).

The four *Spitzer* Infrared Array Camera (IRAC) bands include H₂ lines such as the 1–0 O(5) λ3.235 μm and 0–0 S(13) λ3.8464 μm lines in the IRAC 3.6 μm band, the 0–0 S(1) λ4.181 μm and 0–0 S(9) λ4.6947 μm lines in the IRAC 4.5 μm band, the 0–0 S(7) λ5.5115 μm and 0–0 S(6) λ6.1088 μm lines in the IRAC 5.8 μm band and the 0–0 S(5) λ6.9091 μm and 0–0 S(4) λ8.0258 μm lines in the IRAC 8 μm band. Observations of PNe have shown the relevance of nebular emission in the IRAC 8 μm band as it contains few emission from stars and more intense diffuse emission than the IRAC 3.6 and 4.5 μm bands (e.g. Anderson et al. 2012), while having a better sensitivity than the IRAC 5.8 μm band. Furthermore, the IRAC 3.6 and 4.5 μm bands are dominated by bremsstrahlung emission and by the ionic transition lines of Brα λ4.052 μm, [Mg IV] λ4.49 μm and [Ar VI] λ4.53 μm (Phillips & Ramos-Larios 2010). IRAC 8 μm images of PNe frequently reveal emission from extended haloes and molecular knots (Ramos-Larios & Phillips 2009; Chu 2012; Phillips & Marquez-Lugo 2011). The comparison between IRAC 8 μm and H₂ images of PNe (e.g. NGC 6720 and NGC 7293) reveals an excellent match between the appearance in the two bands that indicates a common origin (Hora 2006; Hora et al. 2006), although molecular hydrogen is suspected, the contribution from the [Ar III] λ8.991 μm line cannot be neglected (Hora et al. 2004).

Accordingly we have searched the *Spitzer* archive for IRAC 8 μm images of PNe showing extended emission that could be attributed to molecular material. The sample, composed of eight morphologically diverse PNe, has subsequently been imaged through narrow-band optical and near-IR filters to ascertain the presence and spatial distribution of ionized material and H₂. Two PNe, namely M1-79 and NGC 6778, were added to this sample as they exhibit intriguing narrow-band optical and near-IR morphologies, despite there

are no *Spitzer* images for them. The comparison between optical, near- and mid-IR images has allowed us to verify the presence of molecular material in regions of H₂ emission, but also from regions where H₂ is shielded from the stellar UV radiation field, so that the H₂ molecules are neither disrupted nor excited. In this paper we present evidence that the bipolar PNe–H₂ relationship is not as close as claimed by *Gatley's rule*, as H₂ emission is found in PNe with morphological types other than bipolar.

The observations and archival data are presented in Section 2. The results for each individual PN are described in Section 3. The discussion and final summary are presented in Section 4.

2 OBSERVATIONS AND ARCHIVAL DATA

2.1 Optical images

Most of the optical images presented in this paper (Table 1) have been obtained at the Observatorio Astronómico Nacional (OAN, Mexico), using either the 1.5-m Harold Johnson or the 0.84-m telescopes. At the 1.5-m telescope, a [N II] filter (λ_c = 6584 Å, Δλ = 11 Å) was used, whereas at the 0.84-m telescope either a [N II]+Hα filter (λ_c = 6564 Å, Δλ = 72 Å) or a [N II] filter (λ_c = 6583 Å, Δλ = 10 Å) was used. The narrow-band [N II] images of M1-79, M2-48, M2-51 and NGC 7048 were obtained using the RUCA filter wheel (Zazueta et al. 2000) at the OAN 1.5-m telescope. The detector was the SITE1 1024 × 1024 CCD with pixel scale 0.252 arcsec pixel⁻¹, binning 2 × 2 and field of view (FoV) 4.2 × 4.2 arcmin². The narrow-band [N II] images of NGC 6563 and NGC 6772 were obtained using the RUCA filter wheel at the OAN 1.5-m telescope with the detector Marconi e2v 2048 × 2048 CCD with pixel scale 0.14 arcsec pixel⁻¹, binning 1 × 1 and 2 × 2, respectively, and FoV 4.7 × 4.7 arcmin². The narrow-band [N II] image of NGC 6537 was obtained using the MEXMAN filter wheel at the 0.84-m OAN telescope with the SITE4 1024 × 1024 CCD that provides a pixel scale of 0.39 arcsec pixel⁻¹, binning 1 × 1 and a FoV of 6.7 × 6.7 arcmin². The [N II]+Hα image of NGC 650-51 was obtained using SOPHIA (Sistema Óptico Para Hacer Imágenes de campo Amplio), an optical system for the acquisition of wide-field images at the 0.84-m OAN telescope. This time, the detector was a 2048 × 4608 CCD e2v, named ESOPPO, providing a pixel scale of 1.07 arcsec pixel⁻¹, binning 1 × 1 and a FoV of ≈30.0 × 30.0 arcmin².

For NGC 6778, we have used the [N II] images published by Miranda, Ramos-Larios & Guerrero (2010). The images were obtained

Table 1. Optical and infrared imaging.

	Optical		H ₂ 2.122 μm	Near-IR		Mid-IR	
	[N II] 6584 Å	R 6600 Å		K _s 2.17 μm	K _c 2.27 μm	W2 4.6 μm	IRAC4 8 μm
A66	...	DSS	NTT	<i>Spitzer</i>
M1-79	1.50 m OAN	...	WHT	...	WHT	<i>WISE</i>	...
M2-48	1.50 m OAN	...	WHT	...	WHT	...	<i>Spitzer</i>
M2-51	1.50 m OAN	2MASS	<i>Spitzer</i>
NGC 650-51	0.84 m OAN	...	WHT	...	WHT	...	<i>Spitzer</i>
NGC 6537	0.84 m OAN	...	WHT	...	WHT	...	<i>Spitzer</i>
NGC 6563	1.50 m OAN	...	WHT	...	WHT	...	<i>Spitzer</i>
NGC 6772	1.50 m OAN	...	WHT	...	WHT	...	<i>Spitzer</i>
NGC 6778	NOT	...	WHT	...	WHT	<i>WISE</i>	...
NGC 7048	1.50 m OAN	...	TNG	...	TNG	...	<i>Spitzer</i>

Notes. 2MASS – Two Micron All Sky Survey; DSS – Digitized Sky Survey; NOT – Nordic Optical Telescope; NTT – New Technology Telescope; OAN – Observatorio Astronómico Nacional; *Spitzer* – *Spitzer Space Telescope*; TNG – Telescopio Nazionale Galileo; WHT – William Herschel Telescope; *WISE* – *Wide-field Infrared Survey Explorer*.

through the narrow-band [N II] filter ($\lambda_c = 6584 \text{ \AA}$, $\Delta\lambda = 9 \text{ \AA}$) using Andalucia Faint Object Spectrograph and Camera (ALFOSC) in its imaging mode at the 2.56-m Nordic Optical Telescope (NOT) of the Observatorio del Roque de los Muchachos (ORM), La Palma, Spain. The e2v 2048×2048 CCD detector used for these observations provides a pixel scale of $0.184 \text{ arcsec pixel}^{-1}$ and a FoV of $6.3 \times 6.3 \text{ arcmin}^2$.

Finally, for A66 we used an *R*-band Second Palomar Sky Survey (POSS-II) image downloaded from the ESO Digitized Sky Survey² (DSS) with pixel scale $\simeq 1.0 \text{ arcsec pixel}^{-1}$.

2.2 Near-IR images

The narrow-band H_2 $\lambda 2.122 \mu\text{m}$ and K_c continuum near-IR images were mainly obtained at the 4.2-m William Herschel Telescope (WHT) of the ORM using Long-Slit Intermediate Resolution Infrared Spectrograph (LIRIS; Acosta Pulido et al. 2003). The detector was a 1024×1024 HAWAII array with plate scale $0.25 \text{ arcsec pixel}^{-1}$ and FoV of $4.3 \times 4.3 \text{ arcmin}^2$. The narrow-band H_2 $\lambda 2.122 \mu\text{m}$ and K_s continuum $\lambda 2.27 \mu\text{m}$ images of NGC 7048 were obtained using Near Infrared Camera and Spectrometer (NICS; Oliva & Gennari 1995) at the 3.5-m Telescopio Nazionale Galileo (TNG) of the ORM. The Rockwell HAWAII 1024×1024 array used for these observations has a projected scale of $0.25 \text{ arcsec pixel}^{-1}$ and a FoV of $4.3 \times 4.3 \text{ arcmin}^2$. The narrow-band H_2 $\lambda 2.122 \mu\text{m}$ image of A66 was obtained using the Son OF Isaac (SOFI) camera (Moorwood, Cuby & Lidman 1998) at the 3.5-m New Technology Telescope (NTT) of La Silla Observatory, Chile. The detector was a 1024×1024 HgCdTe HAWAII array providing in its large field (LF) mode a pixel scale of $0.288 \text{ arcsec pixel}^{-1}$ and a FoV of $4.9 \times 4.9 \text{ arcmin}^2$. Finally, Two Micron All Sky Survey (2MASS) JHK_s images with pixel scale $1.0 \text{ arcsec pixel}^{-1}$ are presented for M2-51.

2.3 Mid-IR images

The mid-IR images used in this paper have been downloaded mostly from the *Spitzer* archives. The *Spitzer* IRAC images of M2-48 and NGC 6537 belong to the Galactic Legacy Infrared Mid-Plane Survey Extraordinaire (GLIMPSE) programme which used IRAC to map the Galactic plane in the range $|l| \leq 60^\circ$, $|b| \leq 1^\circ$ (Fazio et al. 2004). The GLIMPSE images in the IRAC $8 \mu\text{m}$ band used in this paper have a spatial resolution $\simeq 2 \text{ arcsec}$. Similarly, we have used the *Spitzer* IRAC $8 \mu\text{m}$ images of A66 and NGC 7048 (Program ID 30285, *Spitzer* Observations of Planetary Nebulae 2, PI: Giovanni Fazio), NGC 650-51, NGC 6563 and NGC 6772 (Program ID 68, Studying Stellar Ejecta on the Large Scale using SIRTf-IRAC, PI: Giovanni Fazio) and M2-51 (Program ID 50398, *Spitzer* Mapping of the Outer Galaxy, SMOG, PI: Sean Carey). The spatial resolution of these images varies between $\simeq 1.7$ and $\simeq 2.0 \text{ arcsec}$.

No *Spitzer* images are available for M1-79 and NGC 6778. For these nebulae, we have used *Wide-field Infrared Survey Explorer* (*WISE*; Wright et al. 2010) images retrieved from the NASA/IPAC Infrared Science Archive (IRSA). *WISE* is a NASA Explorer Mission to surveys the entire sky at 3.4, 4.6, 12 and $22 \mu\text{m}$, the so-called W1 through W4 bands, with 5σ point source sensitivities

better than 0.08, 0.11, 1 and 6 mJy, respectively. The 40-cm telescope uses HgCdTe and Si:As detectors arrays with a plate scale of $2.75 \text{ arcsec pixel}^{-1}$. The W2 $4.6 \mu\text{m}$ images were downloaded from the *WISE* All-Sky Data Release. The images have angular resolution $\simeq 6.4 \text{ arcsec}$ and astrometric accuracy for bright sources better than 0.15 arcsec .

2.4 Spitzer spectroscopy in the mid-IR

Spectroscopic observation used in this paper was acquired using the Short-Low (SL) module 1 (SL1) and module 2 (SL2) at short ($5.1\text{--}8.5 \mu\text{m}$) and long ($7.4\text{--}14.2 \mu\text{m}$) wavelength, respectively, of the *Spitzer* Infrared Spectrograph (IRS; Houck et al. 2004). The spectra of M2-51 and NGC 6537 were obtained through *Spitzer* Program 45 (Deuterium Enrichment in PAHs; PI: Thomas Roellig) on 2004 June 1 and *Spitzer* Program 50179 (Planetary Nebulae As A Laboratory For Molecular Hydrogen in the Early Universe; PI: Kris Sellgren) on 2008 November 4, respectively.

3 RESULTS

Based on the inspection of the optical images and previous spatiokinematical studies, when available, we have divided our sample into two broad morphological groups: elliptical PNe and bipolar PNe. The first group includes A66, M2-51, NGC 6563, NGC 6772 and NGC 7048, whereas the group of bipolar PNe is composed of M1-79, M2-48, NGC 650-51, NGC 6537 and NGC 6778.

3.1 Elliptical PNe

3.1.1 A66 – PN G019.8–23.7

A66 was included in the list of old, evolved PNe compiled by Abell (1955, 1966). The DSS optical image (blue in Fig. 1, left) shows a roughly spherical, low surface brightness shell of radius $\simeq 118 \text{ arcsec}$. The best quality narrow-band optical images of A66 were presented by Hua, Dopita & Martinis (1998) who described it as a roundish, old PN with a blowout structure towards the north-east. They also reported the presence of radial structures or filaments escaping outwards, and a band of emission in $H\alpha$ and [N II] crossing the central regions and dividing the nebula into two cavities.

The morphology of A66 in the H_2 and IRAC $8 \mu\text{m}$ images highlights the radial structures hinted in optical images. The H_2 image (Fig. 1, right) shows a series of cometary knots that are mostly distributed along a central band and a fragmented ring of radius 133 arcsec broken towards the north-east. There is a clear correlation between these morphological features and those described in optical images: the central band is coincident with that observed in the optical, the ring-like structure encompasses the optical emission and the lack of H_2 emission towards the north-east corresponds with the $H\alpha$ and [N II] blowout.

The IRAC $8 \mu\text{m}$ image (red in Fig. 1, left) shows very similar morphology in the central regions to that of the H_2 image, but its larger FoV reveals emission extending farther out. Indeed, the H_2 cometary knots that overrun the NTT H_2 image stretch out in the IRAC $8 \mu\text{m}$ emission up to radial distances $\simeq 240 \text{ arcsec}$. The central optical nebula is surrounded by a halo of emission in the IRAC $8 \mu\text{m}$ image. The similarities between H_2 and IRAC $8 \mu\text{m}$ emission in the central regions and the identification of some of the outermost features in the IRAC $8 \mu\text{m}$ image with radial knots in the H_2 image strongly suggest that the outermost emission detected in the IRAC $8 \mu\text{m}$ image is produced by H_2 molecules.

² The DSS is an all-sky photographic survey conducted with the Palomar and UK Schmidt telescopes. The Catalogs and Surveys Branch (CASB) is digitizing the $6:5 \times 6:5$ photographic plates using a modified PDS microdensitometer to support *Hubble Space Telescope* (*HST*) observing programs and to provide a service to the astronomical community.

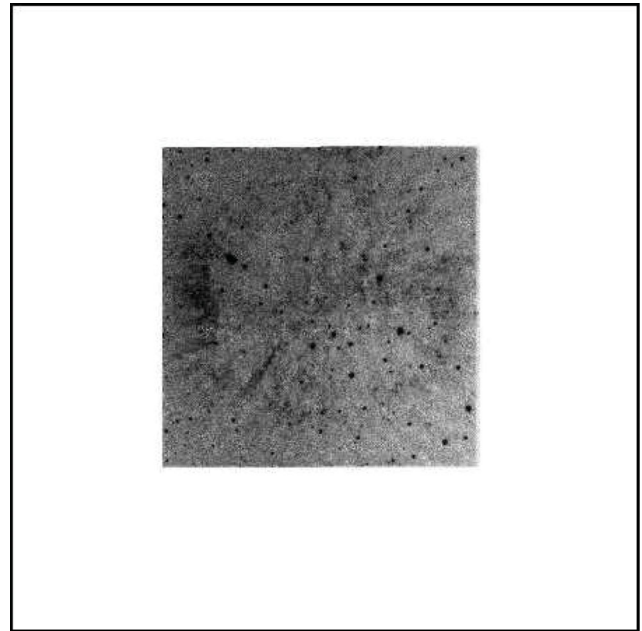
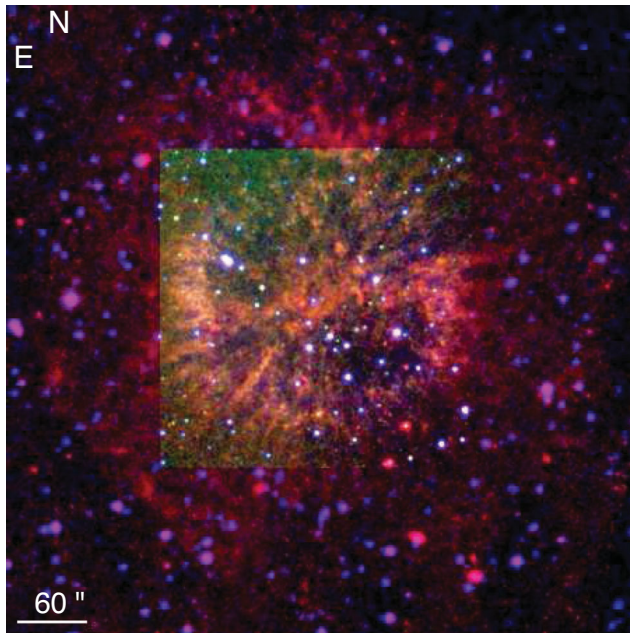


Figure 1. IRAC 8 μm (red), NTT H₂ $\lambda 2.122$ (green) and DSS *R* (blue) colour-composite RGB picture (left), and NTT H₂ $\lambda 2.122$ image (right) of A66. Note the fringing that affects the south-west corner of the H₂ image.

3.1.2 M2-51 – PN G103.2+00.6

Optical [N II] images of M2-51 (Jewitt, Danielson & Kupferman 1986; Balick 1987) have revealed an elliptical morphology with a size $\simeq 36 \times 56 \text{ arcsec}^2$, and major axis almost along the north–south direction. Our [N II] image detects this elliptical shell, as well as an external elliptically shaped outer shell of size $\simeq 60 \times 86 \text{ arcsec}^2$ whose major axis is tilted by $\simeq 30^\circ$ with respect to that of the inner shell. Low surface brightness diffuse emission is also detected along the minor axis of the outer elliptical shell up to a radial distance of 40 arcsec.

No narrow-band observations of the H₂ $\lambda 2.122 \mu\text{m}$ line are available in the literature for M2-51. We have compared the 2MASS *K_s* image with those in the *J* and *H* bands to search for a photometric excess that could be used as a proxy for detection of H₂ emission (see Ramos-Larios, Kemp & Phillips 2006, for details on this technique). The 2MASS image (Fig. 2, right), similar in quality to the *JHK* images presented by Saitō et al. (1999), reveals hints of emission excess from a filamentary structure consistent in size and location with the outer elliptical shell, but the low signal of this emission does not allow us to make a firm statement.

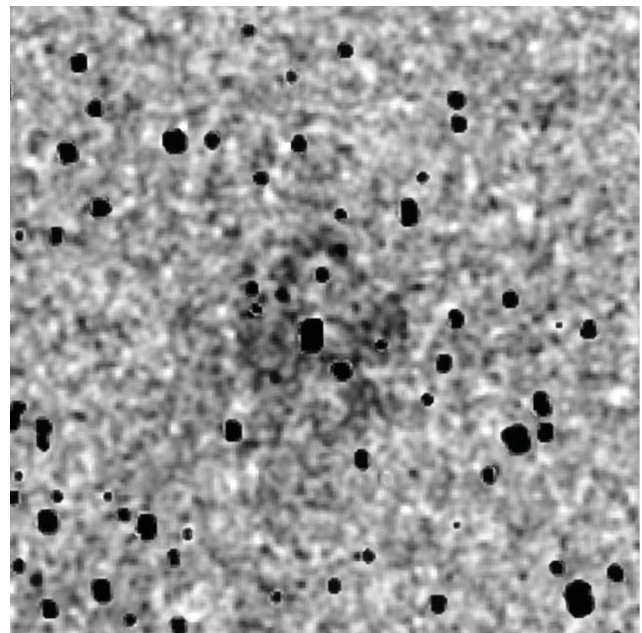
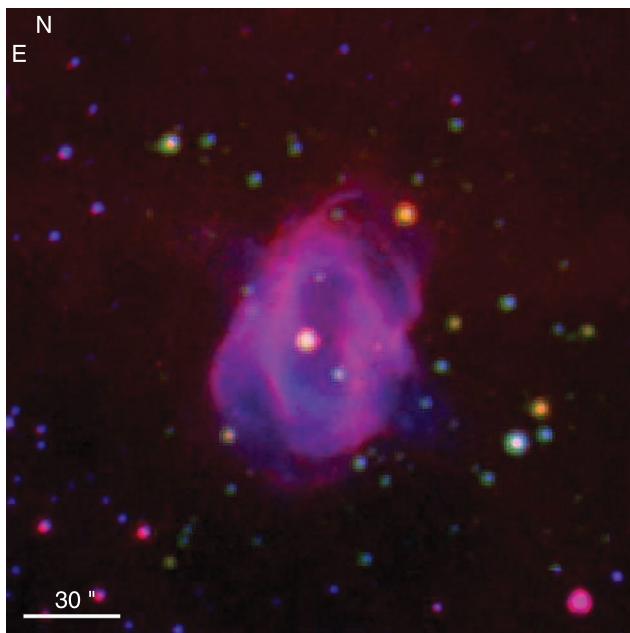


Figure 2. IRAC 8 μm (red), 2MASS *K_s* $\lambda 2.17$ (green) and OAN [N II] (blue) colour-composite RGB picture (left), and 2MASS *K_s* excess image (right) of M2-51.

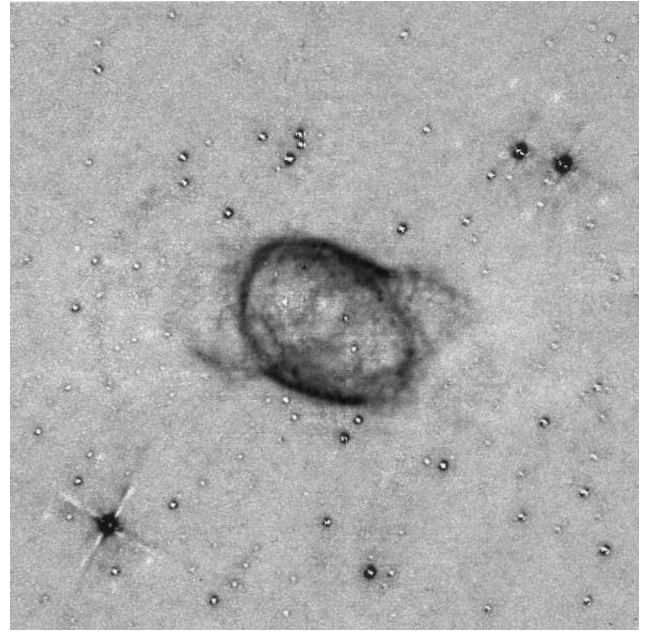
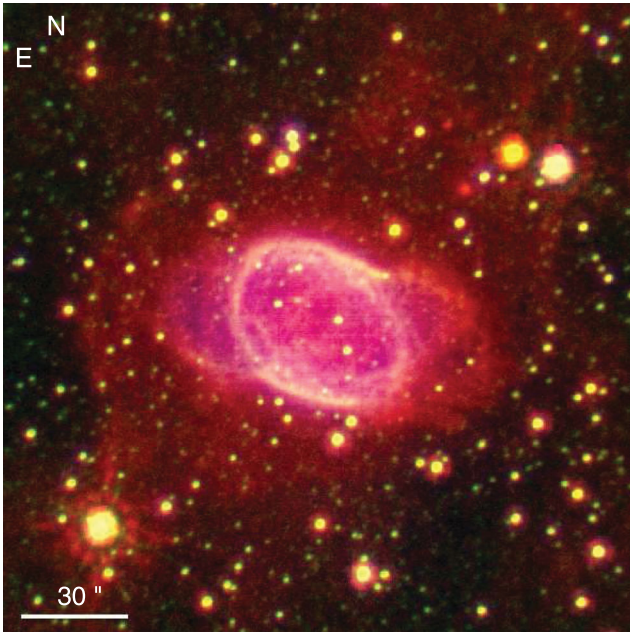


Figure 3. IRAC 8 μm (red), WHT $H_2 \lambda 2.122$ (green) and OAN [N II] (blue) colour-composite RGB picture (left), and WHT continuum-subtracted $H_2 \lambda 2.122$ image (right) of NGC 6563.

The image in the IRAC 8 μm band (red in Fig. 2, left) generally follows the double shell morphology and diffuse emission hinted in the [N II] image. The outer elliptical shell has a size $\approx 80 \times 116 \text{ arcsec}^2$. The ionic or molecular nature of this emission is uncertain.

3.1.3 NGC 6563 – PN G358.5–07.3

NGC 6563 was included in the catalogue of narrow-band images of PNe of Schwarz, Corradi & Melnick (1992). Its $H\alpha + [\text{N II}]$ image displays a main body with elliptical shape and two extensions or *ansae*. Our [N II] image (blue in Fig. 3, left) shows similar elliptical morphology oriented along the north-east–south-west direction [major axis along position angle (PA) $\approx 50^\circ$] with a size of $38 \times 52 \text{ arcsec}^2$. The two *ansae* protrude from the bright inner shell almost along the east–west direction up to radial distances $\approx 40 \text{ arcsec}$. Whereas the optical morphology of NGC 6563 may be interpreted as a wide equatorial belt and narrow bipolar lobes seen almost pole-on, the kinematics do not confirm this interpretation (Vázquez et al., in preparation), but rather confirm an ellipsoidal structure with short, low velocity extensions consistent with *ansae* (Stanghellini, Corradi & Schwarz 1993).

The distribution of molecular hydrogen in NGC 6563 is revealed for the first time in our $H_2 \lambda 2.122 \mu\text{m}$ image (green in Fig. 3, left and Fig. 3, right). The molecular emission outlines that of the elliptical ionized region, both showing a pattern of spiral-like dark lanes and bright filaments. These features are typical of bright ring-like PNe such as the Ring and the Helix Nebula and have been suggested to form part of a tilted barrel-like structure (Speck et al. 2002, 2003; O’Dell, McCullough & Meixner 2004; Meixner et al. 2005). The molecular and ionized emissions in the *ansae*, however, differ notably: in [N II], the emission is uniform, fills the *ansae*, and falls off with radial distance, whereas the H_2 emission encloses the [N II] emission, delineating the *ansae* edges with a remarkable point-symmetric brightness distribution. No H_2 emission is detected outside the bright inner shell along the north–south direction, where the walls of this shell are thicker and may imply more efficient

shielding from the stellar UV radiation. On the other hand, weak, diffuse emission is detected forming a broken, round shell of radius $\approx 50 \text{ arcsec}$. The emission is notably limb brightened along an arc towards the east and north-east, but it appears fuzzy towards the opposite side of the main nebula.

The emission from the bright optical and H_2 shell and *ansae* of NGC 6563 are detected in the IRAC 8 μm image (Fig. 3, left), revealing more clearly the outer shell of size 105 arcsec that surrounds the inner elliptical shell and its *ansae*. This outer shell is well defined along the north-east half, but its appearance is more diffuse in its south-west half. Otherwise, the morphology in the IRAC 8 μm image of the inner shell is similar to that of the ionized and hydrogen molecular material, but there are some subtle differences: the IRAC 8 μm image highlights a pattern of filaments inside the elliptical shell and the *ansae* are both broader and extend further. Whereas the origin of the IRAC 8 μm emission of the inner shell can be attributed to ionized and (most likely) H_2 molecular lines, the nature of the material in the outer shell appears to be H_2 emission, although some contribution of thermal dust emission cannot be excluded (e.g. Phillips et al. 2009).

3.1.4 NGC 6772 – PN G033.1–06.3

NGC 6772 appears in a large number of optical imaging studies of PNe (Jewitt et al. 1986; Jacoby & Kaler 1989; Schwarz et al. 1992; Bachiller et al. 1993; Zhang & Kwok 1998). Our [N II] image (blue in Fig. 4, left) confirms the barrel-like elliptical morphology previously described (e.g. Jewitt et al. 1986). The outer edge of this thick elliptical shell, oriented mostly along the north–south direction, has a size of $31 \times 44 \text{ arcsec}^2$. The shell is distorted along the north-east–south-west direction, where two *ansae* or blisters protrude from the shell. Our [N II] image confirms the presence of outer emission, mostly distributed along the east–west direction, but it also reveals a new structure, an arc of radius $\approx 66 \text{ arcsec}$ towards the east that appears to be one half of an outer round shell.

Previous studies of the spatial distribution of H_2 in NGC 6772 (Webster et al. 1988) showed an elliptical shell distorted towards

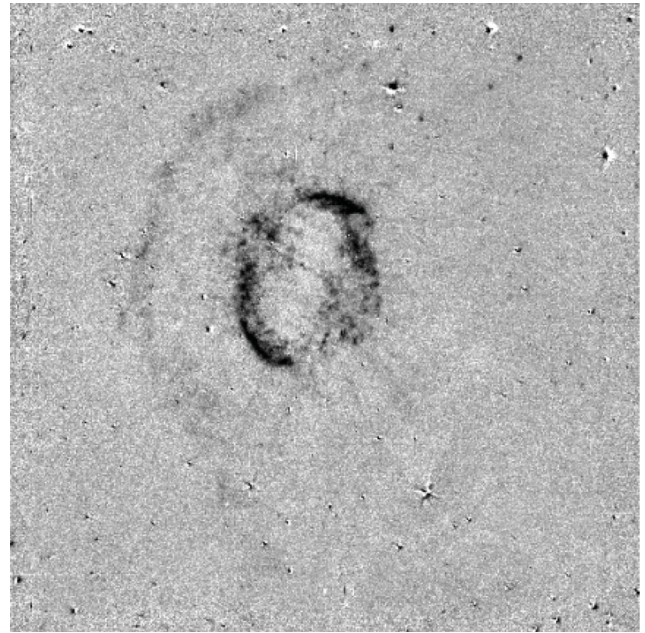
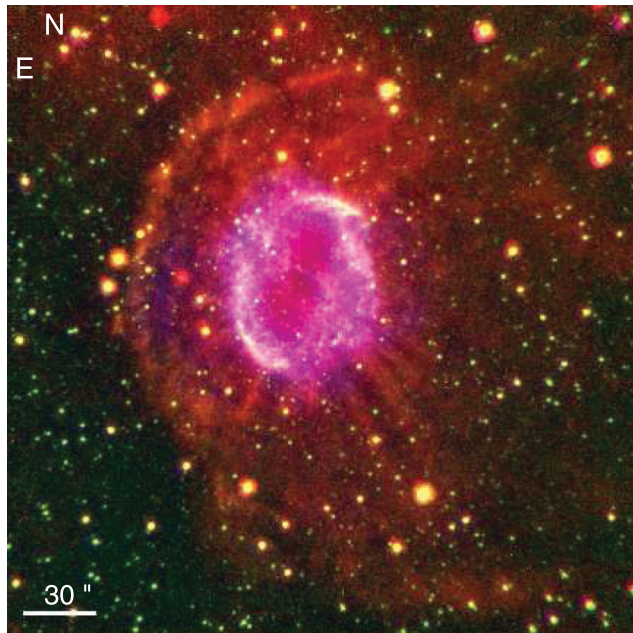


Figure 4. IRAC 8 μm (red), WHT H_2 $\lambda 2.122$ (green) and OAN $[\text{N II}]$ (blue) colour-composite RGB picture (left), and WHT continuum-subtracted H_2 $\lambda 2.122$ picture (right) of NGC 6772.

the north-east and south-west regions. Our H_2 $\lambda 2.122$ image (Fig. 4, right) reveals a wealth of details in this elliptical shell, as well as series of features outside it. The radial features protruding from the inner shell are certainly remarkable. The arc-like feature hinted in the $[\text{N II}]$ images towards the east of the main nebular shell is clearly detected in H_2 with a similar radius, $\simeq 66$ arcsec. This structure has a notable limb-brightness morphology towards the east, whereas it fades and extends further out towards the west. Overall, this morphology is reminiscent of a shell interacting with the interstellar medium (ISM), either by the nebular proper motion or by density gradients in the ISM (Ramos-Larios & Phillips 2009). Similar morphology can be claimed for NGC 6563, but the case of NGC 6772 is certainly more clear.

The IRAC 8 μm emission (red in Fig. 4, left) shows the same spatial distribution than the H_2 emission in the inner elliptical shell, including the distorted regions towards the north-east and south-west. The radial features described in H_2 are also detected in the 8 μm image, but while the H_2 rays are concentrated just outside the inner elliptical shell, in the IRAC 8 μm image the rays are more evenly distributed around the ellipse and extend at greater distances. This coincidence can be interpreted as a common origin for this emission, i.e. molecular hydrogen, whereas the outer section of the rays not detected in the H_2 image may imply that H_2 is present but shielded from UV radiation, so that it is not excited to emit significantly in the 1–0 $\text{S}(1)$ $\lambda 2.122$ line. The outer shell is more clearly revealed in this IRAC 8 μm image than in the H_2 band, with a notable bow-shock morphology towards the north-east. Along the opposite direction, the IRAC 8 μm emission is diffuse and suggests it is trailing the main nebula that would be moving with respect to the ISM.

3.1.5 NGC 7048 – PN G088.7–01.6

Despite being an extended, relatively bright PN, the morphology and physical structure of NGC 7048 have not been studied in detail. The most recent narrow-band optical images mapping its ionized component were presented by Balick (1987) who described it as

a middle elliptical PN, a conclusion also reached in other studies based on the same sets of images (Zhang & Kwok 1998). Our $[\text{N II}]$ image (blue in Fig. 5, left) shows a filamentary, almost round shell of radius $\simeq 30$ arcsec marked by bright eastern and western arcs that leave an opening towards the north and south. Extended emission is detected along these directions at longer radial distances, up to $\simeq 40$ arcsec towards the north and $\simeq 35$ arcsec towards the south. Rather than an elliptical shell, NGC 7048 resembles a tilted barrel that opens at the poles (Frank et al. 1993). Our $[\text{N II}]$ image reveals a weak limb-brightened round shell $\simeq 55$ arcsec in radius that can be described as a halo. This halo is not completely concentric with the bright inner shell, neither its surface brightness is azimuthally constant: the halo has two bright arcs, north and south of the inner shell, along the directions of their polar openings.

The emission in the H_2 $\lambda 2.122$ μm line has been previously described by Kastner et al. (1996) and Davis et al. (2003). Both works report bright H_2 emission from a filamentary barrel-like structure, but the larger FoV images of Kastner et al. (1996) unveil emission along $\text{PA} = 10^\circ$, i.e. mostly along the north–south direction. Indeed, this emission is similar to that shown in our $[\text{N II}]$ image. A close comparison with our H_2 image (Fig. 5, right) confirms these similarities, but it also shows evidences that the diffuse emission emanating through the north and south openings of the inner shell is relatively brighter in the $[\text{N II}]$ line (blue colour in Fig. 5, left). As the spectroscopic study of Davis et al. (2003) for the excitation mechanism of the H_2 emission suggests, the emission from the main shell is shock excited, probably from the propagation of a low-velocity shock generated by the inner shell expanding into the outer halo (Medina et al. 2007).

The IRAC 8 μm image (red colour in Fig. 5, left) follows the H_2 and $[\text{N II}]$ filaments and extended emission of the inner shell of NGC 7048, but where these emissions are faintly detected in the outermost regions, the emission in the IRAC 8 μm band is intense and clearly reveals a round shell of radius $\simeq 56$ arcsec. The emission in this band shows the limb-brightened morphology, but it also discloses radial bright and dark stripes and an azimuthally dependent brightening. These can be associated with the shadowing

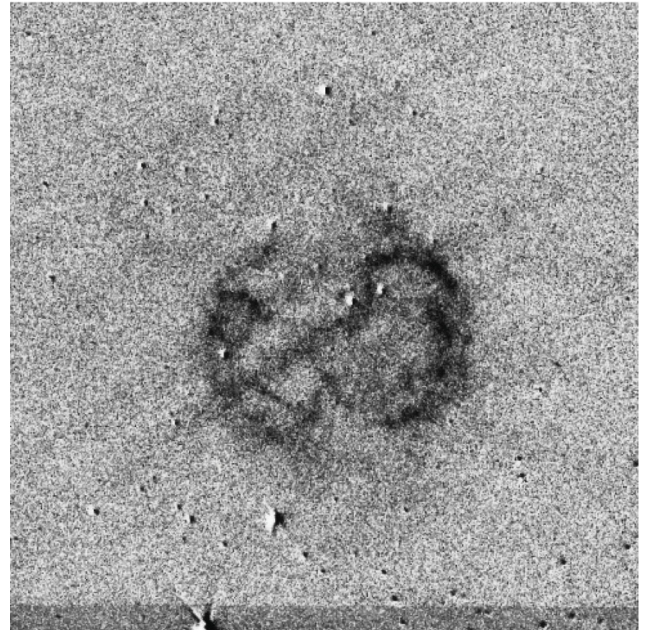
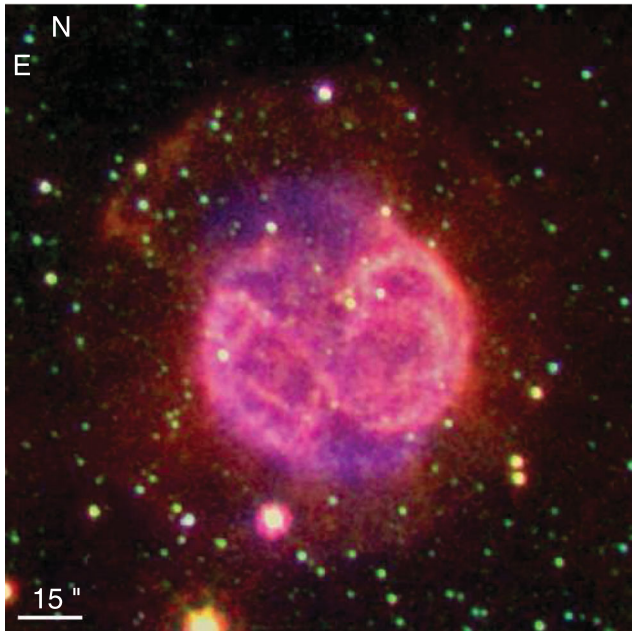


Figure 5. IRAC 8 μm (red), TNG H_2 $\lambda 2.122$ (green) and OAN [N II] (blue) colour-composite RGB picture (left), and TNG continuum-subtracted H_2 $\lambda 2.122$ image (right) of NGC 7048. Note that the background-subtracted H_2 image is affected of fringing that creates a pattern along the south-east–north-west direction.

of the central star by the eastern and western arcs of the inner shell that are most likely optically thick to the UV radiation from the central star, probably in the cooling track of white dwarfs. The correspondence between the H_2 and [N II] features and those in the IRAC 8 μm image suggests that the emission in the inner shell and halo detected in this latter band includes significant contributions of emission lines both from ionized material and molecular hydrogen.

3.2 Bipolar PNe

3.2.1 M1-79 – PN G093.3–02.4

Narrow-band images of M1-79 were presented by Manchado et al. (1996) and its morphology, kinematics and physical structure in optical emission lines of the ionized gas have been extensively studied by Saurer (1997). This latter work describes M1-79 as a $46 \times 24 \text{ arcsec}^2$ bright elliptical shell with its major axis oriented near the east–west direction ($\text{PA} \simeq 85^\circ$). A bright bar crosses the shell at $\text{PA} \simeq 14^\circ$, i.e. this bar is misaligned with respect to the ellipse minor axis and reminds the so-called ‘big-tail’ at the central region of the bipolar PN NGC 2818 (Vázquez 2012). A pair of claw-like features protrude from the bright central region along the south-east–north-west ($\text{PA} \simeq 140^\circ$) direction. A high-contrast image reveals bipolar lobes that extend further out, up to distances $\simeq 45 \text{ arcsec}$.

Our [N II] image (Fig. 6, left) confirms these structural components, additionally revealing that the outer pair of bipolar lobes are tilted with respect to the claw-like features and that there is an even larger north-western bipolar lobe which extends up to $\simeq 65 \text{ arcsec}$. We also detect faint diffuse emission towards the east of the bright inner shell, but there is no clear evidence it takes part of a complete outer shell.

The narrow-band H_2 $\lambda 2.122$ image of M1-79 (green in Fig. 6, left and Fig. 6, right) discloses for the first time the molecular hydrogen distribution in this PN which is in many aspects different from the distribution of ionized material. The outskirts of the optically bright

inner shell are delineated in H_2 , but there are no signs of the bipolar lobes. On the contrary, we detect in H_2 a series of bright radial filaments and shadows emanating from the bright inner shell that, avoiding the directions along which the bipolar lobes are detected, are enclosed within an ellipse of size $\simeq 42 \times 55 \text{ arcsec}^2$. We note that some of the brightest filaments in H_2 are spatially coincident with the diffuse [N II] emission detected towards the east of the bright inner shell. We also note that the bright bar in the inner shell produces a remarkable conical shadow in the H_2 emission, thus suggesting that there is not enough UV flux to excite the H_2 molecules along these directions.

Unfortunately, there are no available *Spitzer* IRAC images of M1-79. We have thus used the *WISE* W2 4.6 μm image to investigate the properties of this nebula at longer wavelengths. This image (red in Fig. 6, left) shows emission from the central regions of M1-79, but the limited spatial resolution and sensitivity of *WISE*, and the possible contribution of near-IR ionic lines to the W2 band are not adequate to study the molecular component of the outer regions of this nebula in this mid-IR image.

3.2.2 M2-48 – PN G062.4–00.2

Different morphological (Corradi & Schwarz 1995; Manchado et al. 1996) and kinematical (Vázquez et al. 2000; López-Martín et al. 2002; Dobrinčić et al. 2008) studies of M2-48 (also known as Hen 2-449) have revealed a highly collimated bipolar PN with an obscured waist, bow-shock features along its major axis and a fragmented off-centre round shell. Our [N II] image (blue in Fig. 7, left) confirms the bow-tie-shaped core with size $\simeq 9 \times 15 \text{ arcsec}^2$ and detects a bow-shock feature east of the main nebula along the major axis at $\simeq 55 \text{ arcsec}$, and two outer bow-shock features $\simeq 95 \text{ arcsec}$ east and $\simeq 120 \text{ arcsec}$ west along an axis tilted by $+5^\circ$ with respect to the bipolar axis of the main nebula. The eastern bow-shock feature at 55 arcsec is coincident with the fragmented round shell that shows a radius of 45 arcsec and is off-centred by 14 arcsec towards the north-east.

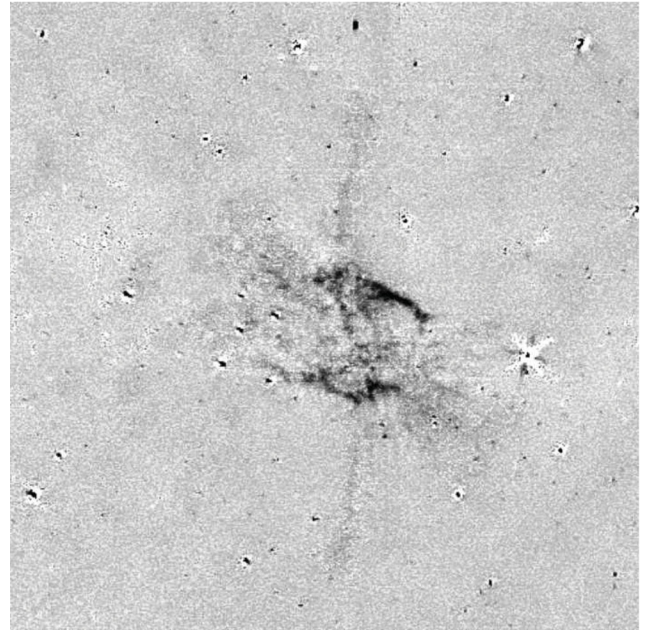
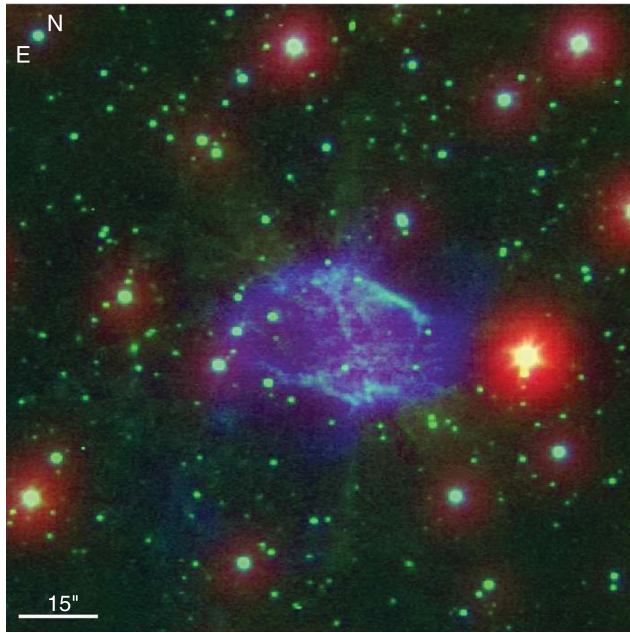


Figure 6. *WISE* W2 4.6 μm (red), WHT H_2 $\lambda 2.122$ (green) and OAN [N II] (blue) colour-composite RGB picture (left), and WHT continuum-subtracted H_2 $\lambda 2.122$ image (right) of M1-79.

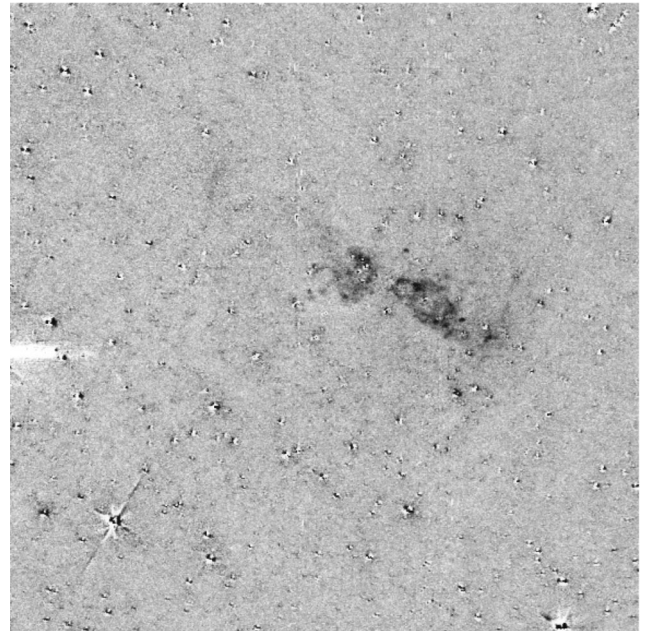
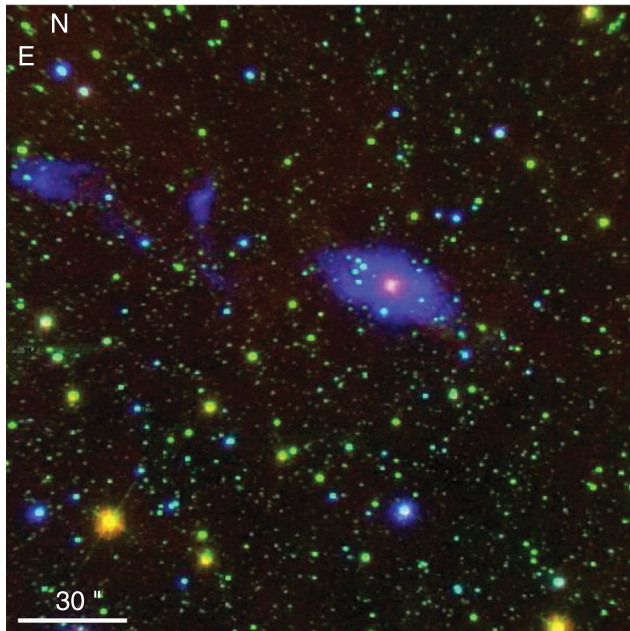


Figure 7. IRAC 8 μm (red), WHT H_2 $\lambda 2.122$ (green) and OAN [N II] (blue) colour-composite picture (left), and WHT continuum-subtracted H_2 $\lambda 2.122$ image (right) of M2-48.

Our H_2 $\lambda 2.122$ image (Fig. 7, right) shows faint emission encompassing the ionized bipolar lobes, but no H_2 emission is detected at the nebular core. There is also even fainter H_2 emission just interior of the brightest eastern and western arcs of the fragmented off-centre round shell, and the eastern bow-shock feature at 55 arcsec. The latter is suggestive of shock excitation of the H_2 molecules at these locations.

The IRAC 8 μm image of M2-48 has been described by Kwok et al. (2008) and Phillips & Ramos-Larios (2008). Here we note that this mid-IR image shows bright emission at the core of the main

nebular shell,³ and faint emission associated with the bipolar lobes. The emission from the bipolar lobes in this image has a biconical morphology and follows more closely the H_2 emission than the [N II] emission, thus indicating that it corresponds to emission from H_2 molecules. No emission at 8 μm seems to be associated with the outer round shell nor to the bow-shock features, but we note that M2-48 is embedded within a region of patchy, diffuse emission.

³ The K_c image used to obtain the continuum-free H_2 image in Fig. 7, right, also shows bright emission at the nebular core.

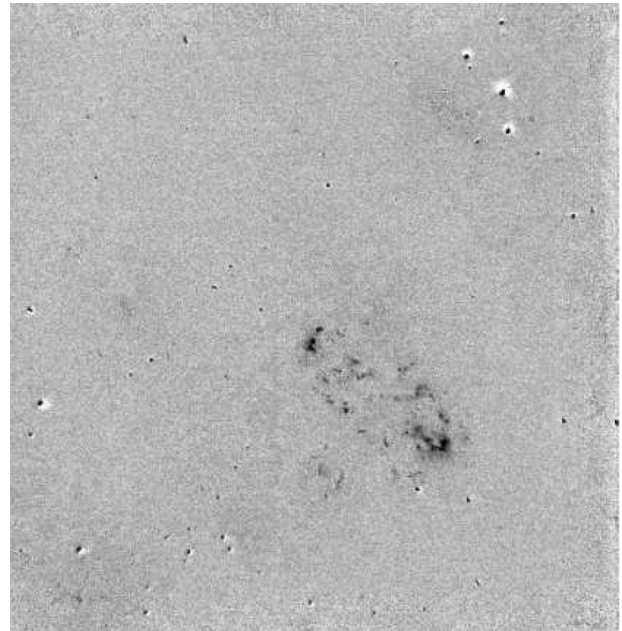
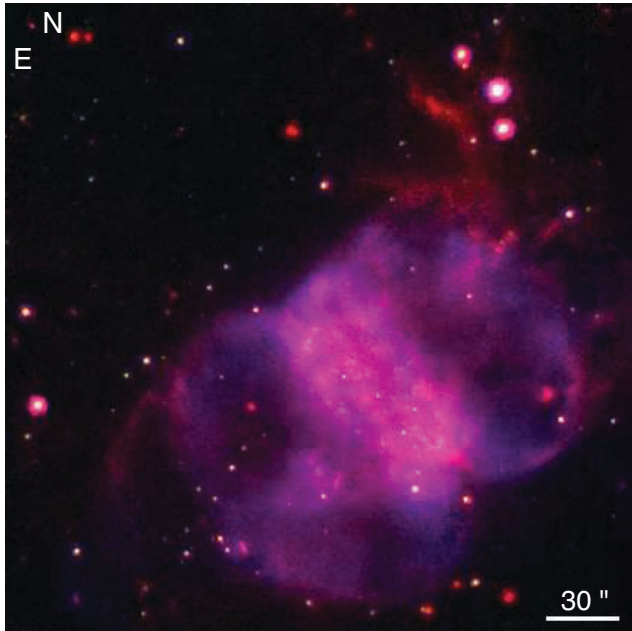


Figure 8. IRAC 8 μm (red), WHT H_2 $\lambda 2.122$ (green) and OAN $[\text{N II}] + \text{H}\alpha$ (blue) colour-composite RGB picture (left), and WHT continuum-subtracted H_2 $\lambda 2.122$ image (right) of NGC 650-51.

3.2.3 NGC 650-51 – PN G130.9–10.5

The optical and mid-IR properties of NGC 650-51 (also known as M76) have been recently studied in detail by Ramos-Larios, Phillips & Cuesta (2008, see also references therein). Our $[\text{N II}]$ image (blue in Fig. 8, left) shows a bright, tilted ring-like structure oriented along the north-east–south-west direction with an angular size of $66 \times 144 \text{ arcsec}^2$. Two bipolar lobes with archetypical butterfly morphology extend along the minor axis of the central ring up to distances $\simeq 85 \text{ arcsec}$. At the tips of these lobes, fainter bow-shaped structures are detected, increasing the total extent of the bipolar lobes up to 260 arcsec.

Previous observations of NGC 650-51 in the H_2 line emphasized the presence of diffuse emission from the central ring, which seemed to be brighter at the tips of its long axis (Kastner et al. 1996). Our H_2 image (Fig. 8, right) resolves this ring into a series of disconnected knots and filaments. Some knots and filaments are also detected in the inner regions of the bipolar lobes.

The spatial distribution of the emission of NGC 650-51 in the IRAC 8 μm image (red in Fig. 8, left) has been compared to those of the ionized and H_2 material (see also Hora et al. 2004; Ramos-Larios et al. 2008). The emission in this mid-IR band closely follows the $[\text{N II}]$ image, showing the central ring, the inner bipolar lobes and their fainter extensions. In addition, the mid-IR emission highlights faint filaments outside the main nebular body.

3.2.4 NGC 6537 – PN G010.1+00.7

NGC 6537 is a high-velocity bipolar PN with a noticeable point-symmetric brightness distribution of the bipolar lobes (Corradi & Schwarz 1993). Narrow-band images obtained with the *HST* confirm these morphological features and also reveal a dust shell at its centre that is suspected to collimate the bipolar lobes (Matsuura et al. 2005). This morphological description is supported by our $[\text{N II}]$ image (blue in Fig. 9, left), in which two bipolar lobes, extending up to 2 arcmin from the centre along the north-east–south-west direction, can be noticed.

The narrow-band H_2 images of NGC 6537 presented by Kastner et al. (1996) and Davis et al. (2003) show strong emission at the nebular core and along an S-shaped line that follows the point-symmetric distribution of the limb-brightened edges of the bipolar lobes. The detection of H_2 emission at the nebular core is uncertain, as K_c images also show bright emission at this location, but the images presented by Davis et al. (2003) seem to confirm a ring-like feature of H_2 emission. Our continuum-subtracted H_2 image (Fig. 9, right) displays this ring, but it also traces the faintest emission from the bipolar lobes. Relatively strong H_2 emission is detected at the tip of the north-eastern bipolar lobe which is otherwise rather faint in the $[\text{N II}]$ image.

The IRAC 8 μm image of NGC 6537 (red in Fig. 9, left; see also Kwok et al. 2008; Phillips & Ramos-Larios 2008) shows a bright unresolved source at the nebular core and faint diffuse emission that traces the inner regions of the bipolar lobes. At least for the north-eastern lobe, its tip is detected in the 8 μm band.

3.2.5 NGC 6778 – PN G034.5–06.7

NGC 6778 had received little attention until the discovery of a binary CSPN (Miszalski et al. 2011) and a disrupted equatorial ring fragmented by fast stellar winds and multiple collimated outflows (Guerrero & Miranda 2012). The $[\text{N II}]$ image (blue in Fig. 10, left, adopted from Guerrero & Miranda 2012) has been compared to the H_2 $\lambda 2.122 \mu\text{m}$ (green in Fig. 10, left) and continuum-subtracted H_2 (Fig. 10, right) images. The H_2 emission traces the brightest $[\text{N II}]$ emission at the tips of the equatorial regions. This spatial distribution is reminiscent of a barrel-like structure and may imply that the object is density bounded along the equatorial plane.

Unfortunately, there are no available *Spitzer* images of NGC 6778. The *WISE* W2 4.6 μm image (red in Fig. 10, left) shows a bright, unresolved source at the location of the central regions of NGC 6778. The limited spatial resolution and sensitivity of *WISE*, and the possible contribution of near-IR ionic lines to the W2 band are not adequate to study the molecular component of the outer regions of this nebula.

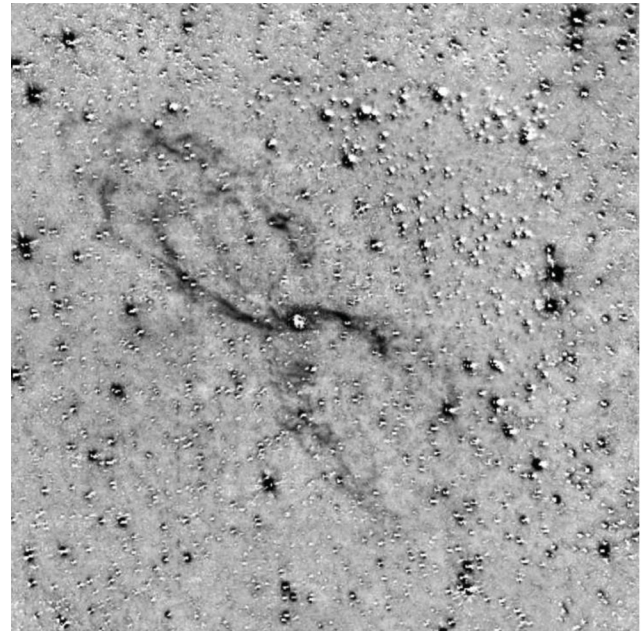
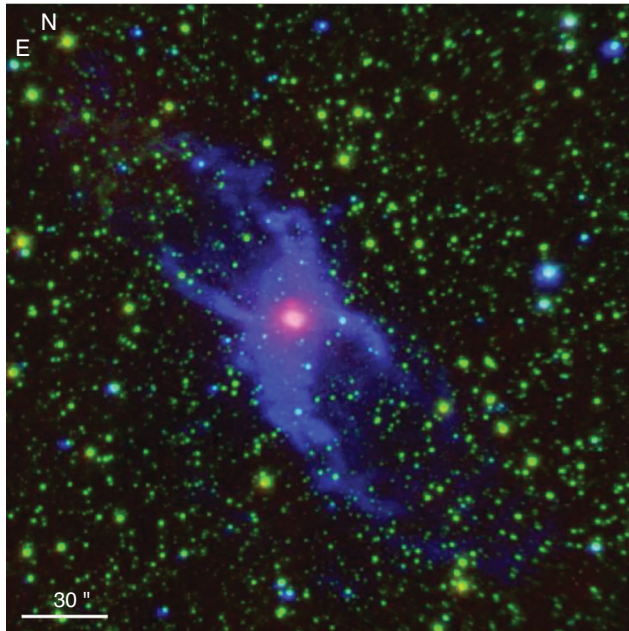


Figure 9. IRAC 8 μm (red), WHT H₂ $\lambda 2.122$ (green) and OAN [N II] (blue) colour-composite RGB picture (left), and WHT continuum-subtracted H₂ $\lambda 2.122$ image (right) of NGC 6537.

4 DISCUSSION

4.1 Interpreting the emission in IRAC 8 μm images

Multiple studies have shown the efficiency of IRAC images in the 8 μm band ($6.2994 \leq \lambda \leq 9.5876 \mu\text{m}$) to detect extended haloes around PNe (e.g., Ramos-Larios & Phillips 2009) and dense knots embedded within ionized nebular shells (e.g. Hora et al. 2006). This emission can be attributed to the contribution into the IRAC 8 μm bandpass of the H₂ 0–0 S(5) $\lambda 6.9091 \mu\text{m}$, 1–1 S(5) $\lambda 7.297 \mu\text{m}$ and 0–0 S(4) $\lambda 8.0258 \mu\text{m}$ rotational lines. However, the contribution of

other emission lines from ionic species, such as [Ar II] $\lambda 6.985 \mu\text{m}$, [Ne IV] $\lambda 7.642 \mu\text{m}$, [Ar V] $\lambda 7.902 \mu\text{m}$ and [Ar III] $\lambda 8.991 \mu\text{m}$, cannot be neglected for the inner ionized nebular regions (Hora et al. 2004). Similarly, the contribution of the polycyclic aromatic hydrocarbon (PAH) features at 6.2, 7.7 and 8.6 μm may be of importance for dusty regions, such as obscured equatorial waists of bipolar PNe and dense knots.

The comparison between H₂ and IRAC 8 μm images of PNe in our sample reveals a close correlation between morphological features seen in the two bands for a significant fraction of sources. The central regions and outermost shells of A66, NGC 6563, NGC 6772

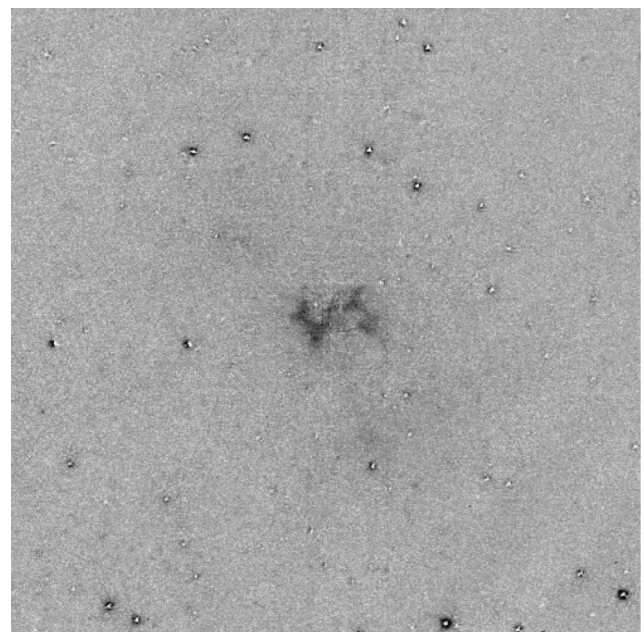
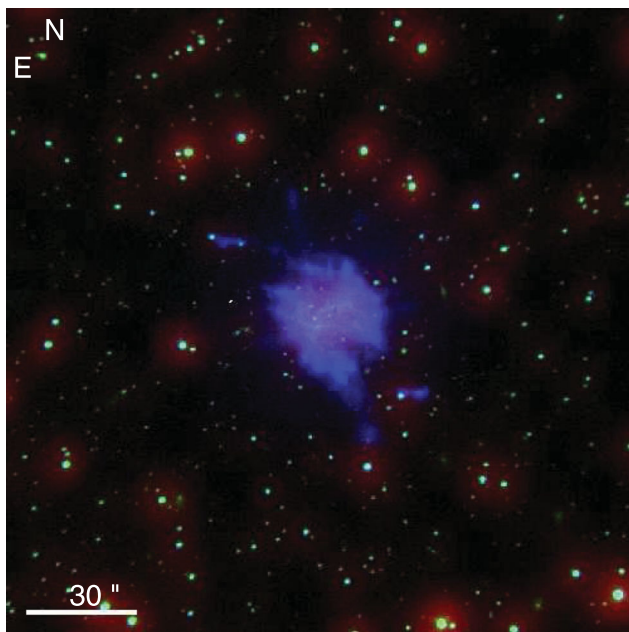


Figure 10. WISE W2 4.6 μm (red), WHT H₂ $\lambda 2.122$ (green) and NOT [N II] (blue) colour-composite RGB picture (left), and WHT continuum-subtracted H₂ $\lambda 2.122$ image (right) of NGC 6778.

and NGC 7048 show overall shapes and detailed morphological features which are very similar in both bands. The H_2 and IRAC 8 μm images of A66 display a fragmentary ring and a series of small-scale structures with an appearance of cometary knots. These knots, whose heads are clearly detected in the innermost regions of A66 mapped by the H_2 image, extend further out in long filaments that are very notable in the larger FoV of the IRAC 8 μm image. Similarly, the inner nebulae of NGC 6563, NGC 6772 and NGC 7048 show an excellent correspondence in the H_2 and 8 μm images, even on small-scale filaments and knots. The H_2 images of these PNe are indicative of limb-brightened, faint outer shells that are brighter and revealed as complete envelopes in the IRAC 8 μm images. These shells, which can be described as haloes (Chu, Jacoby & Arendt 1987), are spatially coincident in the H_2 and 8 μm images. As for A66, there is a series of bright (rays) and dark (shadows) radial filaments that connect the inner and outer shells of NGC 6772.

The similar spatial distribution of the H_2 and IRAC 8 μm images in these PNe suggests that a significant fraction (if not all) of the emission in the IRAC 8 μm images of these PNe can be attributed to lines of molecular hydrogen in this IRAC filter band-pass. This conclusion is supported by the *Spitzer* IRS spectra of NGC 6720 and NGC 7293 which show that the IRAC 8 μm is dominated by H_2 emission lines (Hora et al. 2005, 2006, 2009). To test this suggestion, we have examined the *Spitzer* IRS spectra in the 5.8–8.0 μm band available for the PNe in our sample, namely M2-51 and NGC 6537. The spectra presented in Fig. 11 show that the mid-IR emission in the IRAC 8 μm band from M2-51 and the bipolar lobes of NGC 6537 present prominent H_2 emission of the transitions 0–0 S(5) $\lambda 6.9091 \mu\text{m}$, 1–1 S(5) $\lambda 7.2801 \mu\text{m}$ and 0–0 $\lambda 8.2058 \mu\text{m}$. On the other hand, the mid-IR emission from the central regions of NGC 6537 is dominated by emission lines of ionic species, such as [Ne IV] $\lambda 7.642 \mu\text{m}$ and [Ar III] $\lambda 8.991 \mu\text{m}$, and the PAH feature at 7.7 μm .

We are thus confident that the extended, outermost emission detected in the IRAC 8 μm images can be attributed to H_2 , whereas some contribution of emission lines from ionized material can be expected in the innermost regions. The H_2 emission in the PNe in our sample is mostly associated with shell-like structures and its excitation may be twofold as discussed below.

The H_2 emission is mostly associated with shell-like structures and its excitation may be twofold as discussed below. The inner shell of NGC 7048 is shock excited (Davis et al. 2003), probably associated with the propagation of a small-velocity shock generated by the expansion of the inner shell into the outer shell. The emission of H_2 in the inner shells of NGC 6563 and NGC 6772 may be similarly shock excited, whereas the H_2 emission from the outer shells of A66, NGC 6772 and NGC 7048 seems to exhibit a dependence with ‘openings’ in the inner shell that is suggestive of UV excitation.

Contrary to these nebulae, the spatial distributions of the H_2 and IRAC 8 μm emissions in the bipolar PNe M2-48, NGC 650-51 and NGC 6537 do not correlate closely. The H_2 emission mainly traces the bipolar lobes of M2-48 and NGC 6537, but their IRAC 8 μm images reveal bright emission at their cores, with faint emission from the bipolar lobes. In sharp contrast, the H_2 emission of NGC 650-51 traces its equatorial torus and knotty features in the bipolar lobes, but bright IRAC 8 μm emission also arises from the bipolar lobes.

The lack of *Spitzer* IRAC observations does not allow us to study the relative spatial distributions of H_2 and 8 μm emission for M1-79 and NGC 6778. As for NGC 6772 and NGC 7048, the radial features of H_2 emission seen in M1-79 are indicative of UV

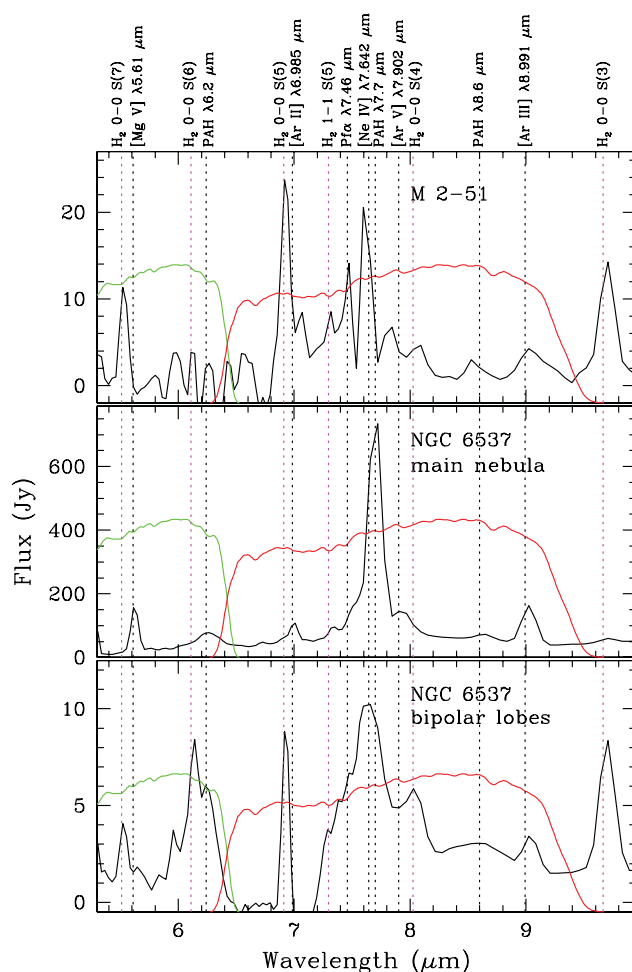


Figure 11. *Spitzer* IRS SL spectra of peripheral region of M2-51 (top) and main nebula region (centre) and bipolar lobes (low) of NGC 6537. The spectra show the IRAC 5.8 μm (green) and 8 μm (red) response profiles. Multiple H_2 and ionic lines and some PAHs bands are marked. There is no definite identification for the bright feature at $\sim 7.6 \mu\text{m}$, especially in the spectrum of the innermost regions of NGC 6537. We note that this is the wavelength at which the SL1 and SL2 spectra joins, thus we cannot discard it is a spurious artefact.

excitation and shielding effects. This may also be the case for the knotty appearance of the equatorial ring of NGC 6778 seen in H_2 .

4.2 Origin of the hydrogen molecular material

The spatial correspondence between H_2 and 8 μm emission can be interpreted by the contribution of H_2 emission lines into the IRAC 8 μm bandpass. Alternatively, the emission in this IRAC band may be attributed to thermal continuum emission from dust coexisting with molecular hydrogen. The spatial coincidence of molecular hydrogen and dust can have important consequences for the origin of the molecular material. The dust may act as a shield for H_2 molecules from the ionizing UV radiation of the star, and thus dust and H_2 may have been present in the nebulae since its formation. Alternatively, the dust grains may act as catalyst for the formation of new H_2 molecules on their surface. These phenomena have been studied by Matsuura et al. (2009) for NGC 7293 (Helix Nebula) and van Hoof et al. (2010) for NGC 6720 (Ring Nebula).

The survival of dense, dusty knots, formed during the AGB phase within the ionized zone is critical for the origin of the molecular material (Redman et al. 2003; García-Segura et al. 2006). If the knots are able to survive a long time, then it can be expected that coeval H₂ has survived shielded from the UV stellar radiation by the high density and relatively low temperature provided by the knots. However, if these dense knots are rapidly destroyed by UV radiation, then the H₂ material detected in old PN should have condensed on to newly formed dust grains.

4.3 H₂ emission and nebular morphology

The literature provides a wealth of observational evidence supporting the prevalence of H₂ emission among bipolar PNe with respect to other morphological types (Kastner et al. 1996, and references therein). Bipolar PNe seem to possess important reservoirs of molecular material, either because they descend from more massive progenitors and have therefore more massive envelopes, or either because the bipolar geometry provides a suitable haven for the survival of molecules in dense equatorial regions. Furthermore, bipolar PNe seem to offer suitable excitation conditions for the excitation and emission of the H₂ molecule, may be through shock excitation, but most likely by offering an appropriate flux of UV exciting photons as the H₂ emission is associated with most cases to UV excitation (Likkell et al. 2006). The quick evolution of the central star of a bipolar planetary nebula – assuming it descends from a massive progenitor – implies it reaches the high effective temperature necessary to provide a suitable UV flux of photons in a short time-scale (Aleman & Gruenwald 2004). The combined effects of post-AGB speed evolution and nebular geometry may indeed play an important role, as bipolar PNe that exhibit an equatorial ring structure have much stronger H₂ emission than bipolar PNe with a narrow waist (Guerrero et al. 2000).

The prevalence of H₂ emission among bipolar PNe led to postulate the so-called *Gatley's rule* (Kastner et al. 1996) stating that ‘the detection of the 2.122 μm S(1) line of H₂ is sufficient to determine the bipolar nature of a PN’. This conclusion was based on the correlation between H₂ detection and bipolar morphology of a sample of PNe, although some of the PNe in that sample exhibiting H₂ emission are not strictly bipolar, i.e. they do not show a butterfly morphology or bipolar lobes connected by an equatorial ring or a waist (Balick 1987; Corradi & Schwarz 1995; Manchado et al. 2000). For example, the physical structure of NGC 6720, the Ring Nebula, has been controverted and sometimes assumed to be bipolar, but a recent study by O’Dell, Sabbadin & Henney (2007) confirms the closed ellipsoidal shape of the inner shell proposed by Guerrero, Manchado & Chu (1997).

The detection of H₂ emission from PNe in our sample with shell-like morphologies (A66, M2-51, NGC 6563, NGC 6772 and NGC 7048) seems to violate *Gatley's rule*. We concur that some of these PNe can be described as ellipsoidal shells with bipolar extensions (e.g. M1-79), or barrel-like structures with shorter extensions or *ansae* (e.g. NGC 6563 and NGC 7048). The kinematical information available for some of them in the literature or in the SPM catalogue (López et al. 2012), however, implies that M2-51, NGC 6563, NGC 6772 and NGC 7048 cannot be described by no means as bipolar PNe. Similarly, the detection of H₂ emission from haloes in A66, NGC 6563, NGC 6772 and NGC 7048 (and probably some more in the literature; e.g. Phillips et al. 2009; Ramos-Larios & Phillips 2009) does not conform *Gatley's rule*.

Even among the bipolar PNe in our sample, we appreciate notable differences. Sources that do not have an equatorial ring (M2-

48 and NGC 6537) show bright 8 μm emission at their cores, but the H₂ emission arises mostly from the bipolar lobes. On the other hand, the H₂ emission from sources with an equatorial ring (NGC 650-51 and NGC 6778) originates from these equatorial regions. In these sources, we note that the H₂ emission does not arise from a torus external to the ionized one, but from dense clumps or knots embedded within the ionized ring. This situation is similar to the H₂ emission detected in NGC 6720 and NGC 7293 (Speck et al. 2002; Hora 2006; Hora et al. 2006; Matsuura et al. 2009; van Hoof et al. 2010), and reminiscent of the knots that occupy the whole volume of the main nebula of NGC 6853 (Manchado et al. 2007) or those that we detect in A66.

Contrary to previous interpretations, the presence of a thick equatorial structure in bipolar PNe does not imply H₂ emission: such structures may provide a haven for the survival of hydrogen molecules, but at the same time UV radiation cannot excite these molecules, and thus H₂ emission is not produced. Meanwhile the H₂ emission from tori of bipolar PNe seems to come from knots that shield themselves from the UV radiation of the central star.

5 SUMMARY

We have compared the emission detected in IRAC 8 μm and near-IR H₂ images to investigate the nature of the emission observed in this mid-IR IRAC band in a sample of PNe. We confirm that a significant fraction of the IRAC 8 μm emission can be attributed to H₂ line emission, thus revealing the molecular nature of the material seen in these IRAC images. The H₂ emission arises from inner shells and outer envelopes or haloes of round and elliptical PNe, as well as from bipolar lobes and dense knots in the equatorial rings of bipolar PNe. We found that H₂ emission is not exclusively associated with bipolar PNe, but objects with a barrel-like physical structure and their haloes have also important amounts of molecular hydrogen. We also suggest that the H₂ emission from equatorial rings of bipolar PNe arises from discrete knots, rather than from a photodissociation region just exterior to the ionized ring.

ACKNOWLEDGMENTS

RAM-L acknowledges support from CONACyT by the CVU 79367 programs ‘Becas Nacionales’ and ‘Becas Mixtas de Movilidad en el Extranjero’. He also acknowledges the Instituto de Astrofísica de Andalucía for its great hospitality and the facilities provided for the realization of this work. GR-L acknowledges support from CONACyT (grant 177864) and PROMEP (Mexico). RV, MAG and GR-L thank support by grant IN109509 (PAPIIT-DGAPA-UNAM). MAG and GR-L acknowledge partial support of the Spanish grants AYA 2008-01934 and AYA 2011-29754-C03-02 of the Spanish Ministerio de Ciencia e Innovación (MICINN) and Ministerio de Economía y Competitividad (MEC) which includes FEDER funds.

This paper based in part on ground-based observations from the Observatorio Astronómico Nacional at the Sierra de San Pedro Mártir (OAN-SPM), which is a national facility operated by the Instituto de Astronomía of the Universidad Nacional Autónoma de México; the Italian Telescopio Nazionale Galileo (TNG) operated on the island of La Palma by the Fundación Galileo Galilei of the Istituto Nazionale di Astrofisica (INAF) at the Spanish Observatorio del Roque de los Muchachos of the Instituto de Astrofísica de Canarias; the William Herschel Telescope, operated on the island of La Palma by the Isaac Newton Group in the Spanish Observatorio del Roque de los Muchachos of the Instituto de Astrofísica de Canarias; the Nordic Optical Telescope, operated on the island of La Palma

jointly by Denmark, Finland, Iceland, Norway and Sweden, in the Spanish Observatorio del Roque de los Muchachos of the Instituto de Astrofísica de Canarias and the New Technology Telescope at the La Silla Observatory.

This publication makes use of data products from the Two Micron All Sky Survey, which is a joint project of the University of Massachusetts and the Infrared Processing and Analysis Center/California Institute of Technology, funded by the National Aeronautics and Space Administration and the National Science Foundation.

Based in part on photographic data obtained using The UK Schmidt Telescope. The UK Schmidt Telescope was operated by the Royal Observatory Edinburgh, with funding from the UK Science and Engineering Research Council, until 1988 June, and thereafter by the Anglo-Australian Observatory. Original plate material is copyright (c) of the Royal Observatory Edinburgh and the Anglo-Australian Observatory. The plates were processed into the present compressed digital form with their permission. The Digitized Sky Survey was produced at the Space Telescope Science Institute under US Government grant NAG W-2166.

This work is based in part on observations made with the *Spitzer Space Telescope*, which is operated by the Jet Propulsion Laboratory, California Institute of Technology under a contract with NASA.

This publication makes use of data products from the *Wide-field Infrared Survey Explorer*, which is a joint project of the University of California, Los Angeles, and the Jet Propulsion Laboratory/California Institute of Technology, funded by the National Aeronautics and Space Administration.

REFERENCES

- Abell G. O., 1955, *PASP*, 67, 258
 Abell G. O., 1966, *ApJ*, 144, 259
 Acosta Pulido J. A. et al., 2003, *ING Newslett.*, 7, 15
 Aleman I., Gruenwald R., 2004, *ApJ*, 607, 865
 Aleman I., Gruenwald R., 2011, *A&A*, 528, A74
 Anderson L. D., Zavagno A., Barlow M. J., García-Lario P., Noriega-Crespo A., 2012, *A&A*, 537, A1
 Bachiller R., Huggins P. J., Cox P., Forveille T., 1993, *A&A*, 267, 177
 Balick B., 1987, *AJ*, 94, 671
 Black J. H., van Dishoeck E. F., 1987, *ApJ*, 322, 412
 Burton M. G., Hollenbach D. J., Tielens A. G. G., 1992, *ApJ*, 399, 563
 Chu Y.-H., 2012, *IAUS*, 283, 21
 Chu Y.-H., Jacoby G. H., Arendt R., 1987, *ApJS*, 64, 529
 Corradi R. L. M., Schwarz H. E., 1993, *A&A*, 269, 462
 Corradi R. L. M., Schwarz H. E., 1995, *A&A*, 293, 871
 Davis C. J., Smith M. D., Stern L., Kerr T. H., Chiar J. E., 2003, *MNRAS*, 344, 262
 Dinerstein H. L., Sterling N. C., Bowers C. W., 2006, in Sonneborn G., Moos H., Andersson B.-G., eds, *Astrophysics in the Far Ultraviolet: Five Years of Discovery with FUSE ASP Conference Series*, Vol. 348, Proceedings of the Conference held 2-6 August, 2004 in Victoria, British Columbia, Canada. Astron. Soc. Pac., San Francisco, p. 328
 Dobrinčić M., Villaver E., Guerrero M. A., Manchado A., 2008, *AJ*, 135, 2199
 Fazio G. G. et al., 2004, *ApJS*, 154, 10
 Frank A., Balick B., Icke V., Mellema G., 1993, *ApJ*, 404, L25
 García-Segura G., López J. A., Steffen W., Meaburn J., Manchado A., 2006, *ApJ*, 646, L61
 Guerrero M. A., Miranda L. F., 2012, *A&A*, 539, A47
 Guerrero M. A., Manchado A., Chu Y.-H., 1997, *ApJ*, 487, 328
 Guerrero M. A., Villaver E., Manchado A., García-Lario P., Prada F., 2000, *ApJS*, 127, 125
 Hora J. L., 2006, in Barlow M. J., Méndez R. H., eds, *Planetary Nebulae in our Galaxy and Beyond*, Proceedings of the International Astronomical Union, Symposium #234. Cambridge Univ. Press, Cambridge, p. 173
 Hora J. L., Latter W. B., 1996, *BAAS*, 28, 1402
 Hora J. L., Latter W. B., Allen L. E., Marengo M., Deutsch L. K., Pipher J. L., 2004, *ApJS*, 154, 296
 Hora J. L., Latter W. B., Marengo M., Fazio G. G., Allen L. E., Pipher J. L., 2005, *BAAS*, 37, 493
 Hora J. L., Latter W. B., Smith H. A., Marengo M., 2006, *ApJ*, 652, 426
 Hora J. L., Marengo M., Smith H. A., Cerrigone L., Latter W. B., 2009, in Sheth K., Noriega-Crespo A., Ingalls J., Paladini R., eds, *The Evolving ISM in the Milky Way and Nearby Galaxies*, The Fourth Spitzer Science Center Conference, Proceedings of the conference held December 2-5, 2007, at the Hilton Hotel, Pasadena, CA. Published online at <http://ssc.spitzer.caltech.edu/mtgs/ismevol>
 Houck J. R. et al., 2004, *Proc. SPIE*, 5487, 62
 Hua C. T., Dopita M. A., Martinis J., 1998, *A&AS*, 133, 361
 Jacoby G. H., Kaler J. B., 1989, *AJ*, 98, 1662
 Jewitt D. C., Danielson G. E., Kupferman P. N., 1986, *ApJ*, 302, 727
 Kastner J. H., Gatley I., Merrill K. M., Probst R., Weintraub D., 1994, *ApJ*, 421, 600
 Kastner J. H., Weintraub D. A., Gatley I., Merrill K. M., Probst R. G., 1996, *ApJ*, 462, 777
 Kwok S., Zhang Y., Koning N., Huang H.-H., Churchwell E., 2008, *ApJS*, 174, 426
 Likkel L., Dinerstein H. L., Lester D. F., Kindt A., Bartig K., 2006, *AJ*, 131, 1515
 López J. A., Richer M. G., García-Díaz M. T., Clark D. M., Meaburn J., Riesgo H., Steffen W., Lloyd M., 2012, *Rev. Mex. Astron. Astrofis.*, 48, 3
 López-Martín L. et al., 2002, *A&A*, 388, 652
 McCandliss S. R., France K., Lupu R. E., Burgh E. B., Sembach K., Kruk J., Andersson B.-G., Feldman P. D., 2007, *ApJ*, 659, 1291
 Manchado A., Guerrero M. A., Stanghellini L., Serra-Ricart M., 1996, *The IAC morphological catalog of northern Galactic planetary nebulae*. Instituto de Astrofísica de Canarias (IAC), La Laguna, Spain
 Manchado A., Villaver E., Stanghellini L., Guerrero M. A., 2000, in Kastner J. H., Soker N., Rappaport S., eds, *Asymmetrical Planetary Nebulae II: From Origins to Microstructures*, ASP Conference Series, Vol. 199, Astron. Soc. Pac., San Francisco, p. 17
 Manchado A., Villaver E., García-Segura G., Acosta-Pulido J.-A., Barrena R., 2007, in *Asymmetrical Planetary Nebulae IV*, held in La Palma June 18-22, 2007. Published online at <http://www.iac.es/proyect/apn4>, article #7
 Matsuura M., Zijlstra A. A., Gray M. D., Molster F. J., Waters L. B. F. M., 2005, *MNRAS*, 363, 628
 Matsuura M. et al., 2009, *ApJ*, 700, 1067
 Medina J. J., Guerrero M. A., Luridiana V., Miranda L. F., Riera A., Velázquez P. F., 2007, in *Asymmetrical Planetary Nebulae IV*, held in La Palma June 18-22, 2007. Published online at <http://www.iac.es/proyect/apn4>, article #33
 Meixner M., McCullough P., Hartman J., Son M., Speck A., 2005, *AJ*, 130, 1784
 Miranda L. F., Ramos-Larios G., Guerrero M. A., 2010, *Publ. Astron. Soc. Aust.*, 27, 180
 Miszalski B., Jones D., Rodríguez-Gil P., Boffin H. M. J., Corradi R. L. M., Santander-García M., 2011, *A&A*, 531, A158
 Moorwood A., Cuby J.-G., Lidman C., 1998, *Messenger*, 91, 9
 O'Dell C. R., McCullough P. R., Meixner M., 2004, *AJ*, 128, 2339
 O'Dell C. R., Sabbadin F., Henney W. J., 2007, *AJ*, 134, 1679
 Oliva E., Gennari S., 1995, *A&AS*, 114, 179
 Peimbert M., Torres-Peimbert S., 1983, in Flower D. R., ed., *Planetary Nebulae*, Proceedings of IAU Symposium No. 103, held 9-13 August 1983 at University College, London, England. D. Reidel Publishing Co., Dordrecht, p. 521
 Phillips J. P., Marquez-Lugo R. A., 2011, *MNRAS*, 410, 2257
 Phillips J. P., Ramos-Larios G., 2008, *MNRAS*, 383, 1029

- Phillips J. P., Ramos-Larios G., 2010, MNRAS, 405, 2179
Phillips J. P., Ramos-Larios G., Schröder K.-P., Contreras J. L. V., 2009, MNRAS, 399, 1126
Ramos-Larios G., Phillips J. P., 2009, MNRAS, 400, 575
Ramos-Larios G., Kemp S. N., Phillips J. P., 2006, Rev. Mex. Astron. Astrofis., 42, 131
Ramos-Larios G., Phillips J. P., Cuesta L., 2008, MNRAS, 391, 52
Redman M. P., Viti S., Cau P., Williams D. A., 2003, MNRAS, 345, 1291
Saitō M., Iwata I., Okumura S.-i., Mori A., Yamashita T., 1999, PASJ, 51, 673
Saurer W., 1997, A&A, 326, 1187
Schwarz H. E., Corradi R. L. M., Melnick J., 1992, A&AS, 96, 23
Speck A. K., Meixner M., Fong D., McCullough P. R., Moser D. E., Ueta T., 2002, AJ, 123, 346
Speck A. K., Meixner M., Jacoby G. H., Knezek P. M., 2003, PASP, 115, 170
Stanghellini L., Corradi R. L. M., Schwarz H. E., 1993, A&A, 276, 463
Turner B. E., Zuckerman B., 1977, BAAS, 9, 591
van Hoof P. A. M. et al., 2010, A&A, 518, L137
Vázquez R., 2012, ApJ, 751, 116
Vázquez R., López-Martín L., Miranda L. F., Esteban C., Torrelles J. M., Arias L., Raga A. C., 2000, A&A, 357, 1031
Webster B. L., Payne P. W., Storey J. W. V., Dopita M. A., 1988, MNRAS, 235, 533
Wright E. L. et al., 2010, AJ, 140, 1868
Zazueta S. et al., 2000, Rev. Mex. Astron. Astrofis., 36, 141
Zhang C. Y., Kwok S., 1998, ApJS, 117, 341

This paper has been typeset from a $\text{\TeX}/\text{\LaTeX}$ file prepared by the author.